Central Lancashire Online Knowledge (CLoK)

Title	Discovery of Potent Multikinase Type-II Inhibitors Targeting CDK5 in the DFG-out Inactive State with Promising Potential against Glioblastoma
Type	Article
URL	https://clok.uclan.ac.uk/51424/
DOI	https://doi.org/10.1021/acs.jmedchem.4c00373
Date	2024
Citation	Khan, Zahra Rafiqa, Welsby, Philip J., Stasik, Izabela and Hayes, Joseph (2024) Discovery of Potent Multikinase Type-II Inhibitors Targeting CDK5 in the DFG-out Inactive State with Promising Potential against Glioblastoma. Journal of Medicinal Chemistry, 67 (9). pp. 7539-7552. ISSN 0022-2623
Creators	Khan, Zahra Rafiqa, Welsby, Philip J., Stasik, Izabela and Hayes, Joseph

It is advisable to refer to the publisher's version if you intend to cite from the work.
https://doi.org/10.1021/acs.jmedchem.4c00373

For information about Research at UCLan please go to http://www.uclan.ac.uk/research/

Discovery of Potent Multi-Kinase Type-II Inhibitors Targeting CDK5 in DFG-out Inactive State with Promising Potential against Glioblastoma

Zahra R. Khan, [a] Philip J. Welsby, [b] Izabela Stasik, [a] Joseph M. Hayes*[a, c]

[a] School of Pharmacy & Biomedical Sciences, University of Central Lancashire, Preston PR1 2HE, United Kingdom

[b] Education Directorate, Royal College of Physicians, Liverpool, L7 3FA, United Kingdom

[c] Biomedical Evidence-based Transdisciplinary (BEST) Health Research Institute, University of Central Lancashire, Preston PR1 2HE, United Kingdom

1

Abstract

Kinases have proven valuable targets in successful cancer drug discovery projects, but not yet for malignant brain tumours where type-II inhibition of cyclin-dependent kinase 5 (CDK5) stabilizing the DFG-out inactive state has potential for design of selective and clinically efficient drug candidates. In the absence of crystallographic evidence for a CDK5 DFG-out inactive state protein-ligand complex, for the first time, a model was designed using metadynamics/ molecular dynamics simulations. Glide docking of ZINC15 biogenic database identified [pyrimidin-2-yl]amino-furo[3,2-b]-furyl-urea/amide hit chemical scaffolds. For four selected analogues (**4**, **27**, **36** and **42**), potent effects on glioblastoma cell viability in U87-MG, T98G, and U251-MG cell-lines and patient-derived cultures were generally observed ($IC_{50}s \sim$ 10-40 µM at 72 h). Selectivity profiling against eleven homologous kinases revealed multi-kinase inhibition (CDK2, CDK5, CDK9 and GSK-3α/β), most potent for GSK-3α in the nanomolar range ($IC_{50}s \sim 0.23–0.98$ µM). These compounds may therefore have diverse anti-cancer mechanisms of action and are of considerable interest for lead optimization.

Keywords: CDK, DFG-out, glioblastoma, GSK-3, kinase, metadynamics, type-II inhibitors

1. Introduction

Glioblastoma (GBM) is the most aggressive malignant brain tumour in adults and has high rates of recurrence. It is associated with very poor prognosis, with <5% of patients surviving 5 years.[1] The current standard of treatment is surgical resection, when possible, and radiotherapy in combination with temozolomide (TMZ), a DNA alkylating agent.[2] Despite these treatment options, GBM survival rates have not changed much in the last three decades. The limited efficacy of current treatment methods and the aggressive nature of this tumour, emphasizes the urgent need for the discovery of alternative treatment strategies.

There are currently > 70 FDA approved kinase inhibitors, mainly for treating cancer. Among the 518 kinases identified in the human genome,[3] cyclin-dependent kinases (CDKs) are known to play significant roles in cell cycle control and regulation of transcription. CDK5 is involved in brain development functions such as neuronal cell survival, synaptic plasticity and neuronal differentiation.[4] However, the expression of CDK5 in glioma tissues is approximately 6-fold higher than in normal brain tissue[5] and dysregulated activity of the kinase contributes towards GBM proliferation and metastasis.[6, 7] Previous studies of CDK5 inhibition for the potential treatment of GBM have shown promise, including the prevention of glioma stem cell (GSC) self-renewal which contribute towards therapeutic resistance.[8] Another study reported the use of a CDK5 inhibitor in concomitant use with TMZ or irradiation, revealing increased DNA damage and a prolonged survival in xenograft mouse models.[9] However, despite these apparent successes, it is unlikely that single kinase inhibition is a viable approach to GBM treatment, in part due to development of treatment resistance and tumour reoccurrence.

Multiple Kinase Inhibitors (MKIs), on the other hand, have potential benefits by targeting a tumour using synergistic effects and overcoming resistance.[10, 11] As an example, dual targeting of CDK-5/-9, where inhibition of CDK5 would affect glioma growth and self-renewal of glioma stem cells,[5, 8] and the inhibition of CDK9 would reduce the generation of mature mRNAs in

3

cells, would in theory block tumour cell proliferation and lead to apoptosis.[12, 13] Importantly, there are numerous approved drugs for other cancers that act as MKIs such as cabozantinib, lenvatinib, pazopanib, sorafenib, sunitinib and vandetanib.[14, 15]

Inhibition of a kinase in the inactive state has attracted considerable interest in recent years, fuelling optimism for new cancer treatments.[16] The majority of reported kinase inhibitors are type-I, binding at the ATP-binding site in the active conformation with the highly conserved kinase Asp-Phe-Gly (DFG) motif of the activation loop orientated towards the binding site (DFG-in). Type-II inhibitors targeting DFG-out (inactive state), exploit interactions with both the ATP-binding site as well as an adjacent allosteric pocket. Type-II inhibitors could be regarded as more advantageous in comparison to ATP competitive inhibitors due to potential for (i) greater selectivity (exploiting allosteric sites)[17] and (ii) better clinical efficacy, linked with longer inhibitor residence times.[18, 19] CDK5 type-II inhibition has not yet been previously directly explored. There is no crystallographic evidence of type-II inhibition of CDK5 and the expectation is that not all kinases have potential for targeting DFG-out inactive state, with the gate-keeper residue being a key determinant.[20] In the case of CDK5, this is a bulky Phe80, however, in a multiple kinase screening of known type-II inhibitors against more than 442 kinases, some CDK5 inhibition was observed for certain compounds (Figure 1), suggesting potential for pursuing this approach.[21]

The contribution of natural products to drug discovery has been recognized for many decades, particularly in the area of cancer,[22, 23] providing optimism for also achieving success against GBM. In this study, Desmond metadynamics (MetaD) and molecular dynamics (MD) simulations were used to predict a CDK5 DFG-out model that allowed *in silico* screening for type-II inhibitors, using molecular docking of natural product based compounds (ZINC15 biogenic database).[24] Predicted candidate (Phase I) inhibitors were experimentally validated using isolated *in vitro* CDK5 binding assays, revealing two low micromolar CDK5 inhibitors

4

with the same hit scaffold. A Phase II set of nineteen analogues were selected for structure-activity relationship (SAR) analysis, revealing ten compounds with IC_{50}s for CDK5 inhibition ranging between 9-60 µM. Four of these ten compounds were tested for their potential against GBM cell-lines (U87-MG, T98G, U251-MG) and short-term patient derived cultures (PD301) revealing promising effects on cell viabilities (IC_{50}s generally < 40 µM). Kinase profiling against homologous kinases revealed the compounds to selectively target kinases that are known targets for GBM, highlighting the potential of identified compounds and their hit chemical scaffold.

Sorafenib	NVP AST-487	BIRB-796
$IC_{50} = 8.3$ µM	$IC_{50} = 0.55$ µM	$IC_{50} = 2$ µM
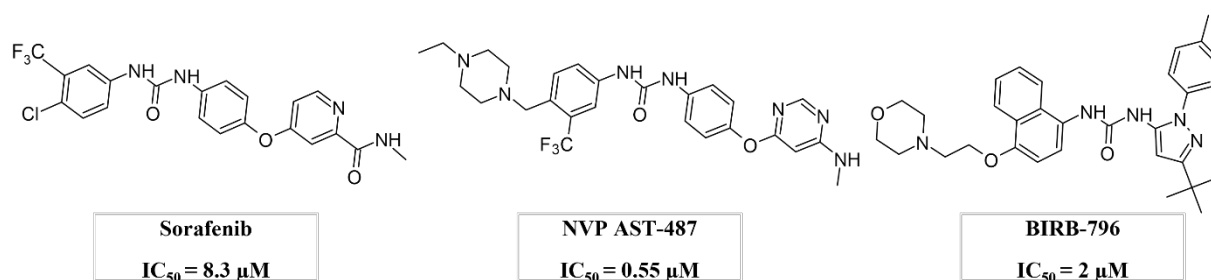
Figure 1. Known type-II inhibitors of CDK5 together with the IC_{50}s, as identified and reported in a comprehensive analysis of type-II inhibitors by Davis *et al.,* 2011.[21]

2. Results & Discussion

2.1 In Silico Studies

2.1.1 Metadynamics DFG-out Model Generation

The DFG-out model of CDK5 was generated using a DFG-in crystallographic complex (PDB: 4AU8) as starting point. One collective variable (CV) was used for Desmond[25] MetaD calculations, defined as the distance between residues Gly113 (α helix) and Phe145 (from DFG activation loop); an equivalent CV selection was successfully applied for generation of a GSK-3β DFG-out model.[26] The 50 ns MetaD simulation revealed the CDK5 DFG activation loop to explore multiple conformations. The DFG-in to -out transformation was observed 21-25ns; this was observed between 10-25 ns for GSK-3β.[26] The transformation of the activation loop, taking the Phe145 side chain out of the binding site, results in access to the hydrophobic allosteric

5

pocket. In this CDK5 DFG-out conformation, the Glu51/Lys33 salt bridge helps stabilize the αC helix and positions Glu51 in the binding site so that its carboxylate side chain is available to form interactions with a putative type-II ligand.[27] For the identified DFG-out conformation from the MetaD simulation (free energy ~5.5 kcal/mol higher than DFG-in), the CV distance between the centre of mass (COM) of the Phe145 sidechain and the $C\alpha$ atom of Gly113 was measured, revealing an increase in distance from 4.5 Å to 18.5 Å for DFG-in to DFG-out state. The activation loops for DFG-in and DFG-out conformations are compared in Figure 2(A) and 2(B), respectively, where the Phe/Asp flip can be seen and the corresponding changes in the loop shape. The DFG-out model adopts a loop conformation qualitatively similar to the model created by Davies *et al.* for GSK-3β.[28] D1 and D2 distance measurements described by Vijayan colleagues can be used to determine if the classical DFG-out conformation has been produced.[27] Specific to CDK5, D1 denotes the distance between the $C\alpha$ atom of Asn131 and Phe145 (DFG loop) and, D2 denotes the distance between the $C\alpha$ atom of Glu51 (αC helix) and Phe145. For the DFG-out conformation, these measurements are observed to be D1 = 7.23 Å and D2 = 12.37 Å, close to agreement with the distances (D1 $\leq$ 7.2 Å and D2 $\geq$ 9.0 Å) proposed by Vijayan and colleagues.[27]
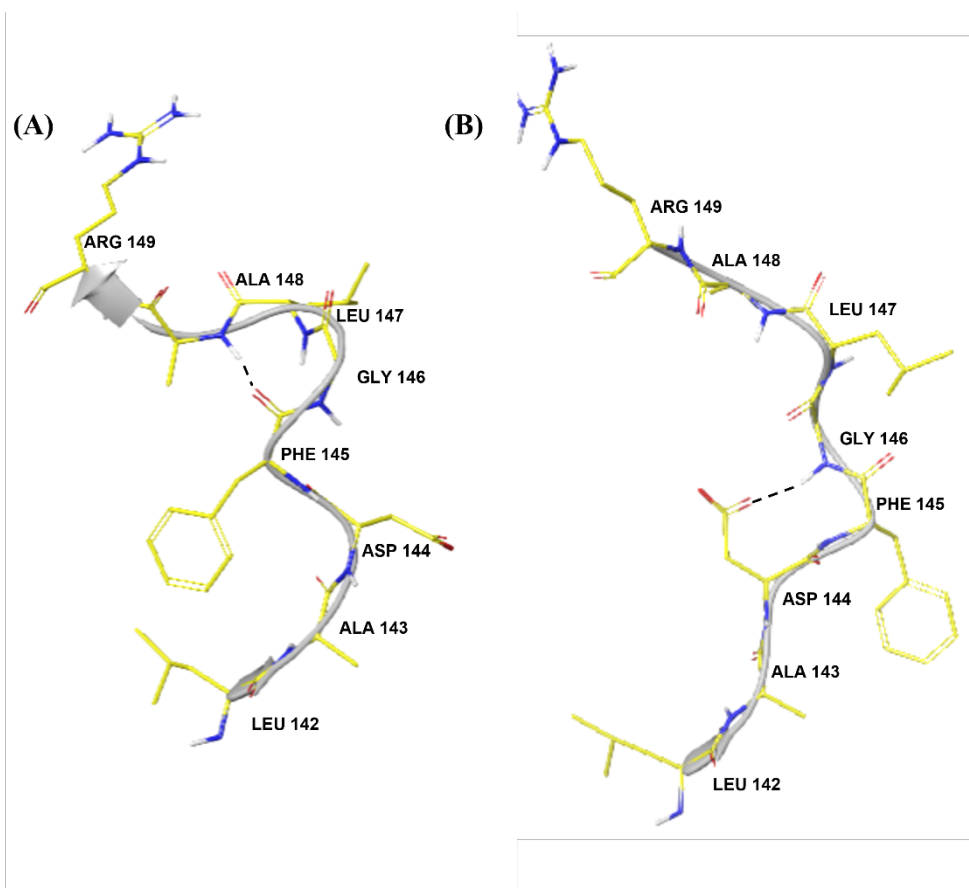
Figure 2. **(A)** The DFG-in activation loop conformation of CDK5 from the original crystal structure (PDB code: 4AU8) compared with **(B)** the metadynamics DFG-out model.

Using the Meta-D DFG-out model, Glide [29] docking of sorafenib (Figure 1) was performed and the stability of the protein-ligand complex analyzed by a 100 ns Desmond molecular dynamics (MD) simulation. After the first 20 ns, the protein backbone and sidechains were equilibrated (RMSD plots included in Figure S1). For the final 80 ns, the trajectory was further analyzed and the occurrence of different protein-ligand interactions displayed in Figure 3. The trajectory frames from the last 80 ns were clustered and the representative taken from the most populated cluster used as the final DFG-out model; binding interactions are shown in Figure 4(A), together with the D1 and D2 measurements for the refined model in Figure 4(B). Classical protein-ligand interactions of a type-II inhibitor [27] formed during sorafenib docking were shown to be stable during the MD simulation: (a) at least one hydrogen bond interaction with the hinge region backbone Glu81 CO and Cys83 CO and NH (b) hydrogen bonding with the Glu51 sidechain

from the αC helix and (c) a hydrogen bond with the DFG loop Asp144 backbone NH. These critical type-II interactions were present throughout > 94% of the simulation (Figure 3), revealing a strong binding affinity between the type-II ligand and the DFG-out model. SiteMap calculations[29] were used to quantify the binding site volumes and revealed values of 232.6 $Å^3$ and 517.9 $Å^3$ for the active and inactive states, respectively. The corresponding increased surface area is consistent with a 'classical' conformation of an inactive kinase which can accommodate type-II inhibitors.[26] A nomenclature for classification of active and inactive kinase structures has been proposed. [30] The system is based on clustering of kinase conformations considering location of the DFG-Phe side-chain and the activation loop orientation (through relevant dihedrals). Using this system and the online-server (http://dunbrack.fccc.edu/kincore/), our designed model had the expected inactive DFG-out BBAminus classification (required for binding type-II inhibitors) with αC-helix-in, further validation of the prediction. The three known type-II CDK5 inhibitors (Figure 1) were also successfully docked to the refined model (including redocking of sorafenib). Glide poses and docking scores (-10.78 – -5.73) of the inhibitors (Table S1) revealed the ability of all three to successfully bind at the site, forming the key protein-ligand interactions. The predicted binding poses of NVP AST-487 and BIRB-796 are included in Figure S2.
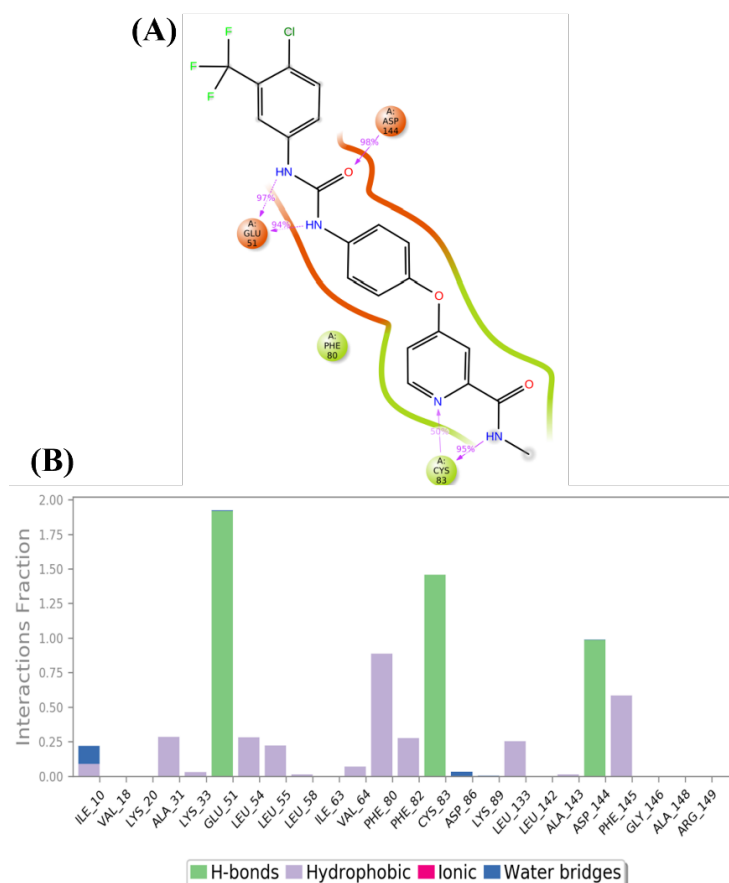
Figure 3. Molecular dynamics simulation of the CDK5-sorafenib complex. **(A)** The prevalence of the interactions between the key protein residues and ligand during the simulation and **(B)** The interaction fraction of a broader range of binding site residues with the ligand.
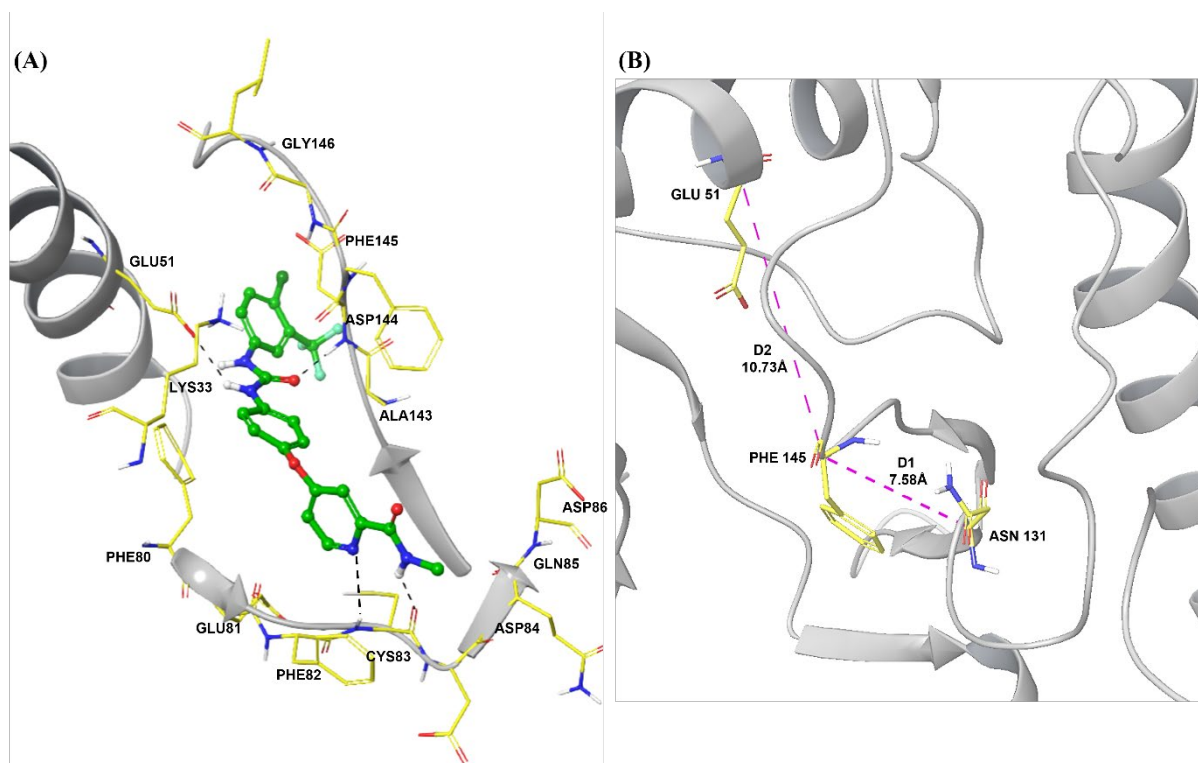
Figure 4. **(A)** The representative structure from the most populated cluster from the molecular dynamics' simulation of the CDK5 – sorafenib complex, used as the final CDK5 DFG-out model. Hydrogen bond interactions between the protein and ligand are shown as black dashed lines. **(B)** D1 and D2 measurements of this final DFG-out model are close to consistent with Vijayan and colleagues' benchmark values (D1 ≤ 7.2 Å; D2 ≥ 9.0 Å) to accommodate a type-II inhibitor.[27] D1 is slightly larger than the suggested value, but this was also previously observed for a predicted GSK-3β – sorafenib DFG-out model.[28]

An initial doubt regarding the potential for DFG-out model creation was the bulky gatekeeper residue Phe80 which could prevent access to the allosteric pocket. Previous literature has suggested that smaller gatekeeper residues are more likely to accommodate type-II ligands and are possibly a prerequisite for type-II inhibition.[20] The conformational analysis by Vijayan *et al*. in 2015 investigated the gatekeeper residues for the type-II inhibitor bound complexes and found only 5% contained Phe as the gatekeeper, therefore, demonstrating it to be less common.[27] The created CDK5 DFG-out model here demonstrates that CDK5 can accommodate type-II inhibitors and Phe80 does not impede this. In fact, favourable hydrophobic/π-π protein-ligand interactions involving Phe80 with sorafenib are observed (Figure 3).

2.2 Virtual Screening of the biogenic database

The ZINC15 biogenic database was prepared for screening using LigPrep; QikProp was used to generate their predicted ADME profiles. After preparation, a total of 206,974 unique compounds underwent Glide docking to the created CDK5 DFG-out model. 77,770 compounds were returned after docking, and analysed by docking score, ranking and visual inspection of predicted protein-ligand interactions. For the latter, an emphasis on key hydrogen bond formation, ligand shape and occupancy of the binding site was considered. Based on this, twenty-three structurally diverse candidate inhibitors (compounds **1-23**, Figure 5) were selected for Phase I *in vitro* CDK5/p35 binding assay experiments; for some chemical scaffolds, more than one analogue was selected to reduce potential for missed hits. The docking scores and predicted activity ranks of the Phase I (and Phase II) compounds are shown in Table S2. The

phase I selection was mainly from the top 1% (11 compounds) or top 5% (17 compounds) of the ranked database.

2.3 *In Vitro* Isolated Enzyme Binding Assays

2.3.1 Phase I Compounds

The twenty-three selected Phase I candidate inhibitors were validated in an CDK5/p35 isolated enzyme binding assays, initially at single 50 μM concentrations to determine the percentage inhibition, with the best compounds (> 50 % inhibition) taken forward for IC_{50} determination. The results of this are shown in Table 1. Two hit compounds **3** and **4** were revealed with IC_{50}s in the low micromolar range (13.9 μM and 9.8 μM, respectively). Both compounds shared the same scaffold, [pyrimidin-2-yl]amino-furo[3,2-b]-furyl-urea, previously revealed as a scaffold for GSK-3β type-II inhibition.[28] The predicted binding poses of the two hit compounds are presented in Figure 6(B) and 6(C), showing that both compounds span across the ATP-binding site and into the hydrophobic allosteric pocket; a schematic representation of the key structural groups of a type-II inhibitor [31] are shown for hit compound **4** in Figure 6(A), used as a basis for discussion of the predicted protein-ligand binding interactions. All classical type-II protein-ligand interactions are present for both compounds. In the hinge region, there are hydrogen-bond interactions from the ligand 2-aminopyrimidine (hinge region binding group) with Glu81 backbone O and Cys83 backbone NH; the ligand urea groups (hydrogen bonding region) are involved in hydrogen bonds with Asp144 backbone NH (activation loop) and Glu51 sidechain carboxylate (αC helix). While the tail group (phenyl) of **3** extends into the now accessible hydrophobic pocket, the extra -CH_2- of compound **4** allows the phenyl ring at the tail to occupy the pocket deeper. This is accompanied by a flip in the urea of **4** from trans-trans to trans-cis,[32, 33] predicted to facilitate better the hydrogen bonding of the type-II hydrogen bonding group. The hit [pyrimidin-2-yl]amino-furo[3,2-b]-furyl-urea scaffold was further investigated through selection of a Phase II set of analogues (Figure 7), from the original docking for *in vitro*

11

CDK5/p35 binding assays and structure activity relationship (SAR) analysis. All of the selected Phase I and II compounds did not result in warnings for Pan Assay Interference Compounds (PAINS), as determined using the ZINC on-line filter (http://zinc15.docking.org/patterns/home/).
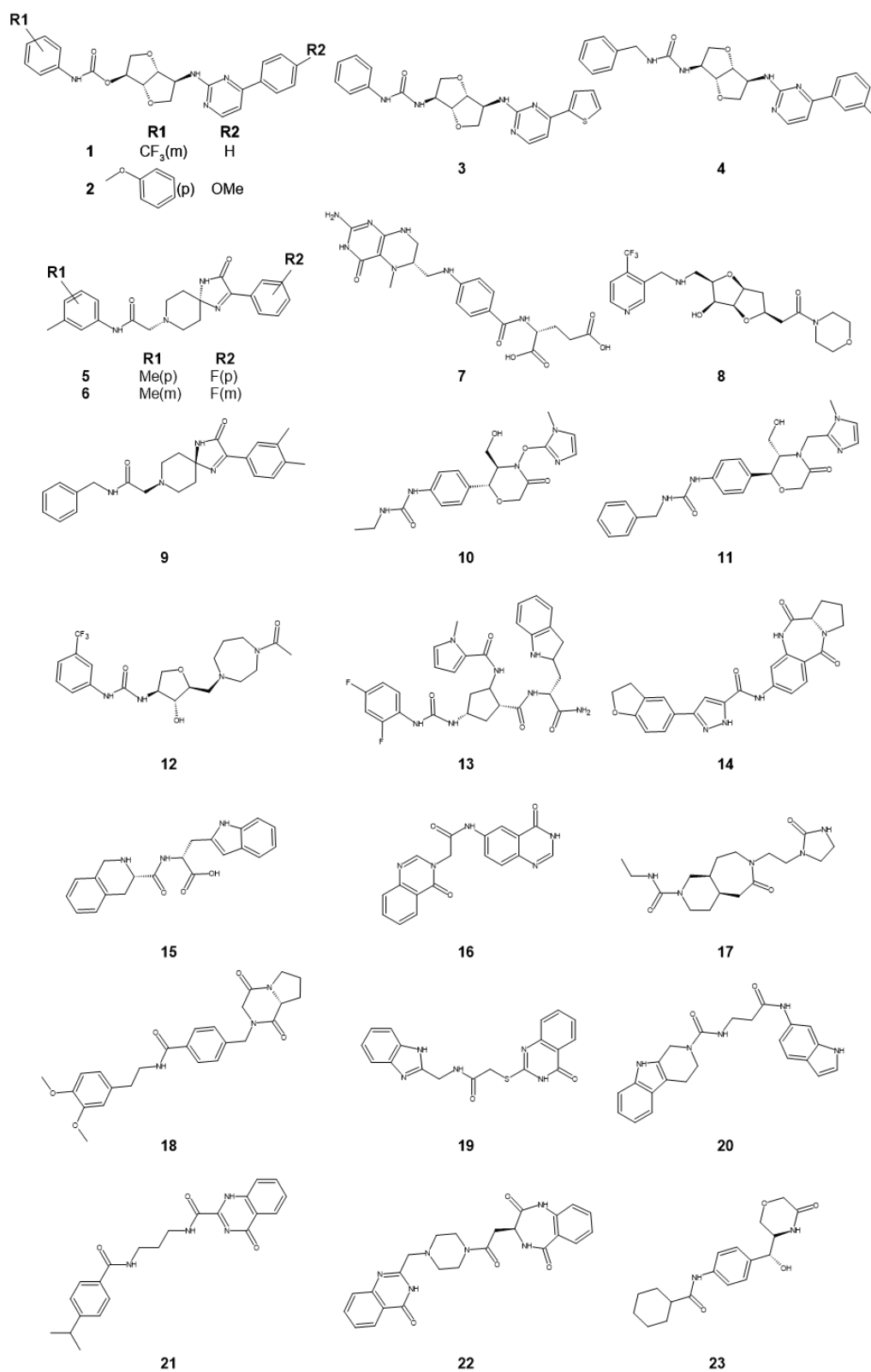
Figure 5. Phase I type-II inhibitor candidates (**1**–**23**) selected for validation using isolated *in vitro* CDK5/p35 binding assays. The IUPAC names of the compounds are included in the Supporting Information.

13

Table 1. Experimental *in vitro* CDK5/p35 binding assay results for the Phase I and II selected type-II inhibitor candidates.[a]

Phase I Compounds [b]				Phase II Compounds [c]			
Compound	IC$_{50}$ (µM) (% inhibition at 50 µM)	Compound	IC$_{50}$ (µM) (% inhibition at 50 µM)	Compound	IC$_{50}$ (µM) (% inhibition at 50 µM)	Compound	IC$_{50}$ (µM) (% inhibition at 50 µM)
1	(14.1%)	13	(14.1%)	24	(15.5%)	36	**15.0 ± 1.1**
2	(6.2%)	14	(1%)	25	(40.2%)	37	**22.5 ± 2.6**
3	**13.9 ± 0.59**	15	(11.7%)	26	(3.5%)	38	**51.5 ± 0.2**
4	**9.8 ± 2.29**	16	(9.7%)	27	**9.8 ± 0.5**	39	(18.2%)
5	(1.9%)	17	(7.1%)	28	**40.3 ± 4.4**	40	(23.8%)
6	(3.7%)	18	*(NI)*[d]	29	(36.5%)	41	**56.1 ± 8.6**
7	*(NI)*[d]	19	*(NI)*[d]	30	**23.8 ± 5.6**	42	**17.8 ± 1.4**
8	(5.4%)	20	*(NI)*[d]	31	(27.9%)		
9	(20.6%)	21	(8.4%)	32	**18.4 ± 0.7**		
10	*(NI)*[d]	22	(14.2%)	33	(41.2%)		
11	(3.2%)	23	(6.6%)	34	(35%)		
12	*(NI)*			35	**26.9 ± 6.5**		

[a] Data reported as IC$_{50}$ (bold font) for the most potent inhibitors and % inhibition at 50 µM (in parentheses) for the other compounds. [b] *c.f.* Figure 5. [c] *c.f.* Figure 7. [d] No inhibition
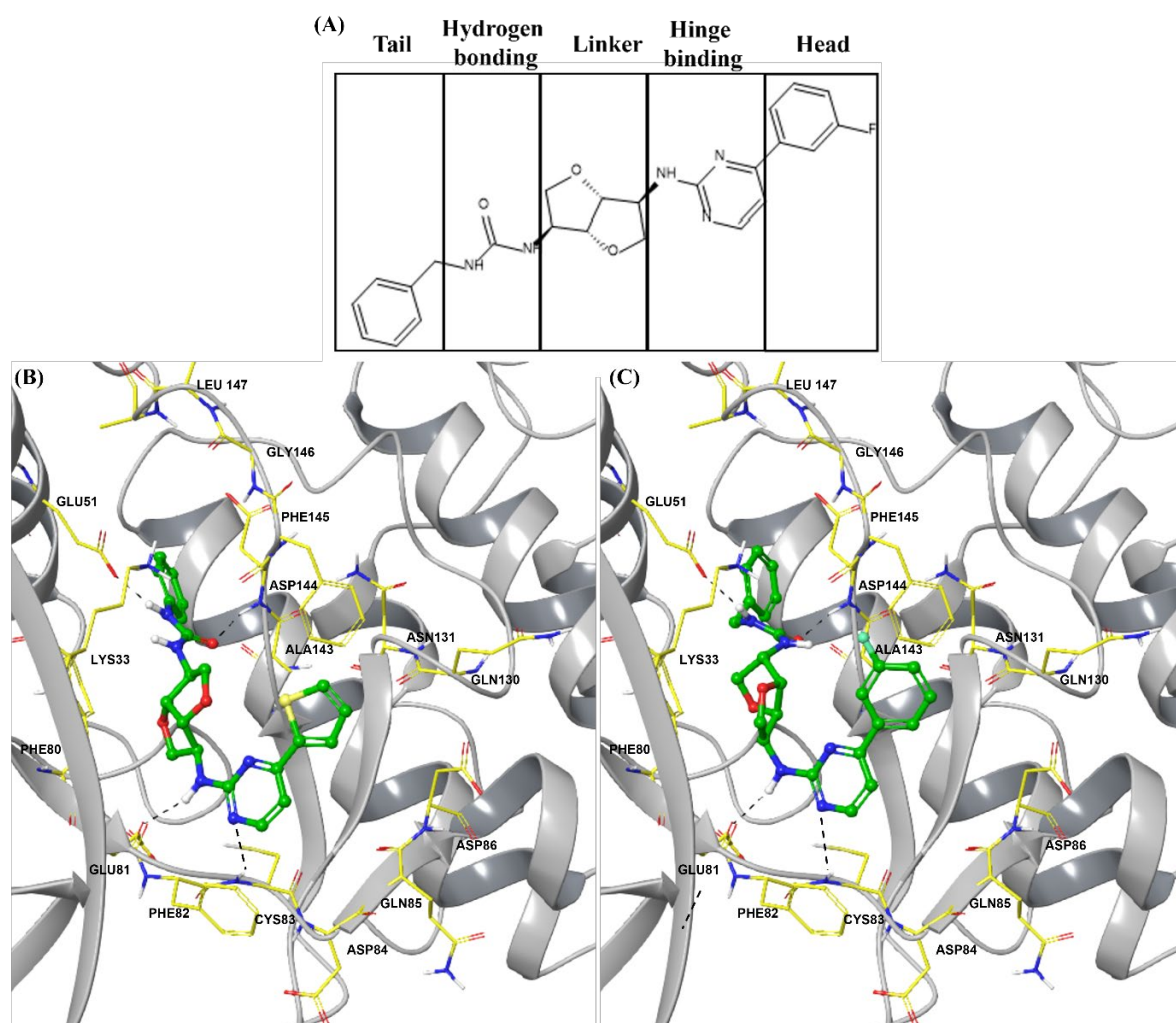
Figure 6. (A) Schematic representation of type-II inhibitor binding groups for the Phase I hit compound **4**. In **(B)** and **(C)**, the Glide-SP predicted binding interactions of the Phase I two identified low micromolar inhibitors from docking to the designed CDK5 DFG-out model are shown: **(B)** compound **3** (IC$_{50}$ = 13.9 μM) and **(C)** compound **4** (IC$_{50}$ = 9.8 μM). Hydrogen bond interactions between the protein and ligand are shown as black dashed lines.
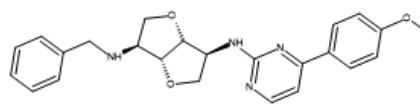
2.3.2 Phase II Compounds

Nineteen Phase II analogues (compounds **24–42**, Figure 7) were selected based on hit compounds **3** and **4** for binding assay and SAR analysis. The CDK5/p35 single concentration (50 μM) binding assay screen revealed that ten of these compounds had inhibition > 45%, and these were selected for IC$_{50}$ determination which ranged between 9–56 μM (*c.f.* Table 1). The key structural groups/features of a type-II inhibitor (Figure 6(A)) are again used as a basis for discussion of the predicted protein–ligand interactions below.
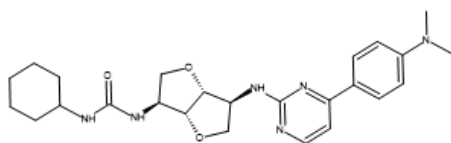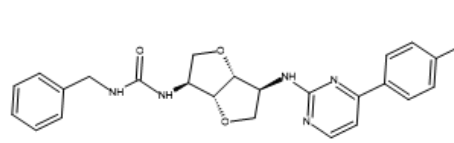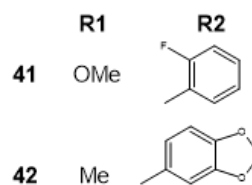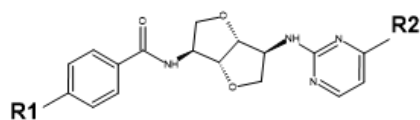
15
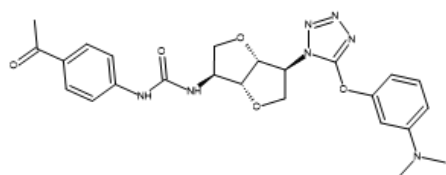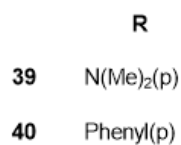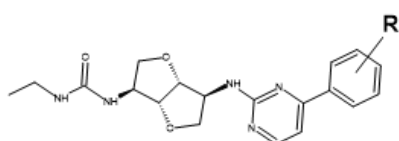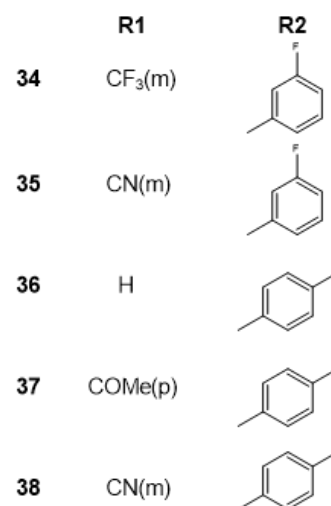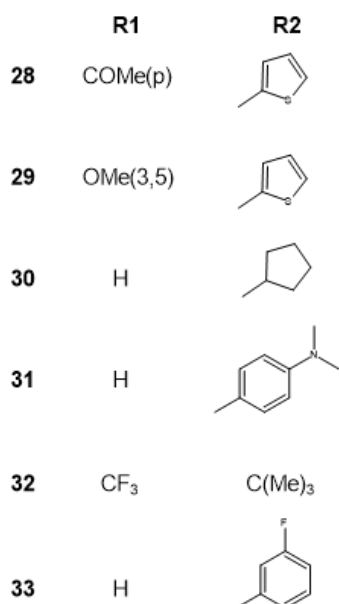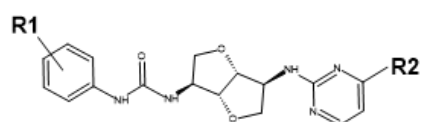
Figure 7. Chemical structures of the Phase II compounds (**24 - 42**) selected for *in vitro* CDK5/p35 binding assays and SAR analysis.

16

The most potent from the Phase II set of compounds was revealed to be compound **27** (IC_{50} = 9.8 μM). Compared to **36** (IC_{50} = 15 μM), compound **27** has an extra -CH_2- before the phenyl group in the tail of the compound, showing a positive effect on potency. This allows the phenyl group to extend further into the hydrophobic allosteric pocket (similar to hit compound **4** from Phase I).

The effect of substituting the urea group in the ligand hydrogen bonding region was probed by comparing compound **25** with **27**. The absence of a urea group for **25**, which instead has an NH group revealed a negative effect on potency, with only 40% inhibition observed in the single concentration 50 μM screen. The lack of the C=O group prevented the crucial hydrogen bonding interaction with the Asp144 backbone in the DFG-out model; additionally, the second NH of a urea has also potential for hydrogen bond interactions with the αC helix Glu51 side chain. In theory, only one ligand NH is required to bind with the Glu51 sidechain, together with a C=O group to bind with the Asp144 backbone NH for the classical type-II interactions. Therefore, **41** and **42** that have an amide group rather than a urea in the hydrogen-bonding region were investigated, with these protein-ligand interactions predicted. The potencies of both these compounds remained good (**41**, IC_{50} = 56.1 μM and **42**, IC_{50} = 17.8 μM), particularly **42**. with a ~3-fold better potency compared to compound **41**.

Compounds **28-38**, analogues of hit compound **3** (IC_{50} = 13.89 μM), allow more in-depth investigation of potential beneficial substitutions at the R1 tail and R2 head groups. In particular, compounds **28**, **30**, **32**, and **35-38** were revealed to be among the most effective compounds with IC_{50}s 15-40 μM. Comparing compound **28** with **37** (IC_{50} = 22.5 μM), where both have the same tail group (para COMe), the methoxyphenyl head group of **37** compared to thiophene of **28** benefits the potency almost 2-fold. Comparing **35** (IC_{50} = 26.9 μM) and **38** (IC_{50} = 51.5 μM) revealed that the R2 head substitution of **35** (meta-fluorophenyl) is more favourable to the para-methoxyphenyl substitution of **38**. Interestingly, compound **30** with a

17

cyclopentyl ring head group was revealed to be one of the most potent compounds ($IC_{50} = 23.8$ μM) from the Phase II screen. This cyclopentyl group is able to exploit favourable van der Waals interactions in the ATP-binding pocket; similar interactions have been proposed as a differential factor for increased binding affinity of CDK5 candidate inhibitors.[34] This observation is consistent with the performance of **32** ($IC_{50} = 18.4$ μM), with an alkyl head-group in the form of -$C(Me)_3$ also favourable.

Compounds **33** (41.2% inhibition at 50 μM), **34** (35% inhibition at 50 μM) and **35** ($IC_{50} = 26.9$ μM) have the same R2 head group (meta-fluorophenyl), allowing an investigation into the R1 substituted phenyl tail groups of these compounds H, CF_3 (meta) and CN (meta), respectively. **35**, with the CN (meta) substituent was indicated as the most potent. Compounds **36** ($IC_{50} = 15$ μM), **37** ($IC_{50} = 22.5$ μM) and **38** ($IC_{50} = 51.5$ μM) also shared the same R2 head group, in this case para-methoxyphenyl; thus, we could also observe the effect of the R1 substituted phenyl tail groups of these compounds (H, COMe (para) and CN (meta), respectively). In this case, the unsubstituted phenyl was found to be the most potent. Compounds **28** ($IC_{50} = 40.3$ μM) and **29** (36.5% inhibition at 50 μM) both have a thiophene group in the R2 position (head group), but the potency of **28** is greater, indicating that R1 = COMe (para) is preferential to OMe (3,5).

Some of the compounds that were found to perform poorly included compound **24** (15.5% inhibition at 50 μM) with a tetrazole hinge binding group, highlighting the importance of the 2-amino-pyrimidine group in this position for all other ligands. For **24**, **26** and **39**, the presence of the substituted phenyl $N(Me)_2$ (para) caused an unwanted flip in the predicted docking orientation consistent with the poor inhibitions observed (< 20% inhibition at 50 μM). Compounds **39** (18.2% inhibition at 50 μM) and **40** (23.8% inhibition at 50 μM) lacked a ring group at the tail of the inhibitor, suggesting its importance within the allosteric hydrophobic pocket.

18

To summarise the SAR study, compounds **4** and **27** were identified as the most potent inhibitors with the extra -CH_2- moiety facilitating deeper access into the hydrophobic pocket. In addition to this, an unsubstituted phenyl group at the tail of the ligand was observed in four of the six most potent compounds (< 20 µM). Our results strongly point towards the presence of a urea group at the hydrogen bonding region to be most effective, although an amide group is worthy of further investigation. Likewise, the iso-propyl R2 substitution of **32** or variations in the cyclopentyl ring of compound **30** in the head group could be explored further.

2.3.3 Kinase Selectivity Screen

To probe the potential selectivity of the discovered type-II CDK5 inhibitors, the most potent compound from Phase I (compound **4**, IC_{50} = 9.8 µM)) and the three most potent compounds from the Phase II screen (compounds **27**, IC_{50} = 9.8 µM; **36**, IC_{50} = 15 µM; and **42**, IC_{50} = 17.8 µM) were investigated further. These four prioritized compounds were first further analyzed by *in silico* docking, for their potential to also bind to the DFG-in conformations (prepared PDB code: 4AU8); it is possible for some kinase inhibitors bind to different states of the same kinase. [30] The docking revealed that the ligands did give poses. However, because the allosteric pocket was inaccessible for DFG-in, to enable hinge region hydrogen bonding the compounds generally had a flipped binding orientation with the ligand head groups interacting with sidechain of the Phe80 gate-keeper residue. The docking scores were inferior (range for four compounds was -4.9 – -7.1) compared to those for the DFG-out conformation (-7.6 – -9.4). A selectivity screening of the four compounds against eleven homologous kinases (GSK-3α, GSK-3β, CDK2, CDK9, PKA, PKBα, PKBβ, PKCα, PKCγ, ERK1 and, ERK2) was next performed at a single concentration (50 µM) and is presented in Figure 8.

19
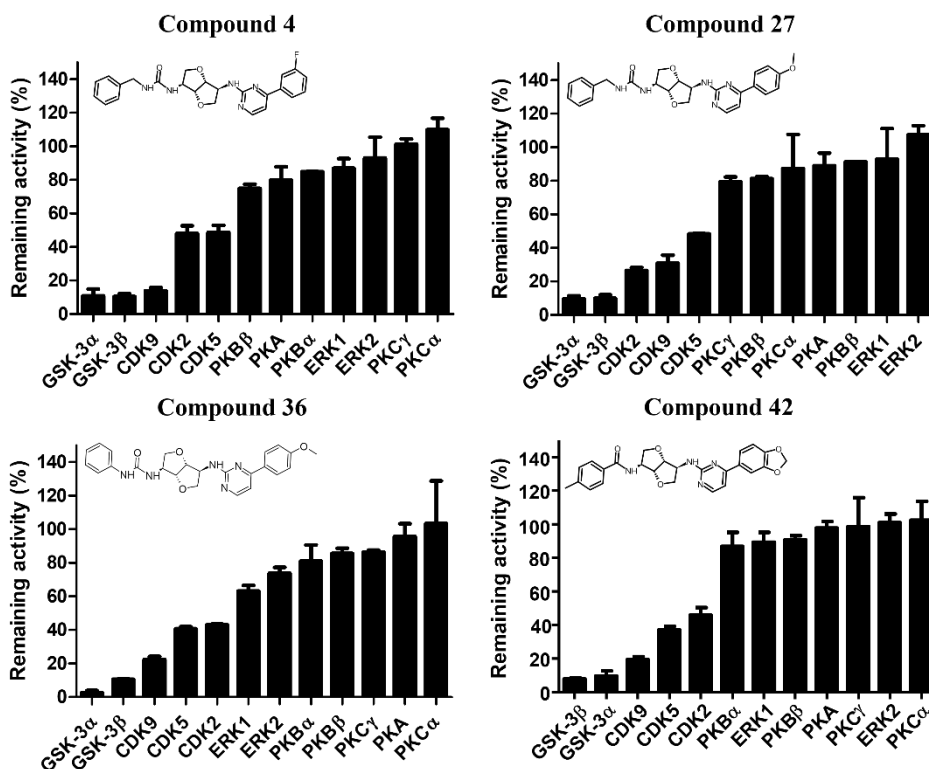
Figure 8. Single-dose (50 μM) selectivity profile of the four selected CDK5 inhibitors (compounds **4**, **27**, **36** and **42**) versus eleven homologous kinases shown as the % remaining activity ± standard deviation.

The single-concentration panel screen highlighted a selective effect of the four compounds against GSK-3α/β, CDK2, CDK5 and CDK9; the kinases for which poor inhibition was observed is potentially due to the formation of DFG-out being less favorable and/or structural differences in the allosteric sites (or binding sites in general). The compounds, therefore, act as multi-kinase inhibitors, but significantly against kinases all of which all have been implicated in GBM.[12, 35-39] The IC_{50}s of the four compounds against these kinases were then determined (Table 2). All four type-II inhibitors were revealed to potently inhibit GSK-3α in the nanomolar range (IC_{50} ~ 0.23 – 0.98 μM). The compounds were low micromolar inhibitors (IC_{50}s < 5 μM) for CDK9 and GSK-3β, but also had IC_{50}s generally < 20 μM for CDK2 (similar to those for CDK5). CDK2 and GSK-3β have previously been established as favourable kinases for type-II inhibitor development.[26, 28, 40] Previous focus on GSK-3 as a therapeutic target has been directed mainly towards the GSK-3β isoform, which has been implicated in many cancers as

20

well as neurological disorders such as Alzheimer's Disease (AD).[41-43] GSK-3β plays a multitude of roles in GBM with effects on proliferation, migration and glioma stem cells.[39] GSK-3α has been studied little in comparison but has been validated to be of considerable importance in brain function, contributing to the worsening of AD as well as cancers such as neuroblastoma, reducing proliferation when inhibited.[44-46] Isoform selective GSK-3α inhibitors have until recently proved difficult to achieve;[47] the four inhibitors reported here are more selective for the α isoform, compound **36** by a factor of almost 6. Both CDK2 and CDK5 have a high sequence similarity determining selectivity[48] and the IC_{50}s for both these kinases are quite similar, particularly for compounds **4** and **36**.

Table 2. IC_{50} determination of the four type-II candidate compounds **4**, **27**, **36** and **42** against CDK/p35, GSK-3α, GSK-3β, CDK9 and, CDK2.

Compound	IC_{50} (μM)				
	CDK5/p35	GSK-3α	GSK-3β	CDK9	CDK2
4	9.8 ± 2.29	0.98 ± 0.09	4.00 ± 1.38	1.76 ±0.35	6.24 ± 2.83
27	9.8 ± 0.51	0.73 ± 0.15	2.70 ± 0.35	2.60 ± 0.27	21.92 ± 2.47
36	15.0 ± 1.11	0.23 ± 0.21	1.29 ± 0.29	2.80 ± 0.09	15.83 ± 2.09
42	17.8 ± 1.38	0.71 ± 0.14	1.95 ± 0.47	3.02 ± 0.36	9.73 ± 5.31

2.4 *In Vitro* Glioblastoma Assays

The four selected compounds (**4**, **27**, **36** and **42**) taken forward for the kinase selectivity profiling were also tested using *in vitro* cellular studies (cell viability) with three established GBM cell lines (U87-MG, T98G and U251-MG) as well as a patient derived, short-term culture PD301. Roscovitine [CY-202, (R)-Roscovitine, Seliciclib] an orally available CDK inhibitor that has undergone clinical trial studies for cancer was also included for comparative purposes.[49] The IC_{50}s for each compound were determined at 24-, 48- and 72-hours (Table 3). For each compound, a time- and concentration-dependent effect on the cell viabilities was generally observed. For compounds **27**, **36**, and **42**, a similar trend was observed with IC_{50}s following 72

21

hours incubation in the range of 12-36 µM across the cell lines. These were similar to values obtained for Roscovitine ($IC_{50}s$ = 15-19 µM). For compound **4**, the $IC_{50}s$ were recorded as slightly higher, ranging between 37 and 87 µM across all cell lines. The cell viability results of the four compounds are better compared to those often reported for TMZ using glioblastoma cell lines such as U87-MG and U251-MG *in vitro*, where IC_{50} values have been in the high micromolar range.[50] However, TMZ is a prodrug that requires metabolic activation under physiological conditions, with *in vitro* results being variable.[51]

Table 3. IC_{50} values for the three glioblastoma cell lines, U87-MG, T98G, and U251-MG, and primary glioblastoma culture, PD301, following 24-, 48-, and 72-hour treatments with control Roscovitine and compounds **4**, **27**, **36** and **42**.

Cell line	IC_{50} (µM)		
	24hr	48hr	72hr
Roscovitine			
U87-MG	64.5	21.0	16.9
T98G	25.0	12.2	18.5
U251-MG	21.8	22.5	15.4
Compound 4			
U87-MG	93.4	91.9	86.7
T98G	91.7	32.9	37.4
U251-MG	91.2	58.4	42
PD301	128.5	68.6	56.4
Compound 27			
U87-MG	83.2	44.7	30.3
T98G	47.2	9.6	11.7
U251-MG	114.5	30	23
PD301	588.3	73.8	28.1
Compound 36			
U87-MG	83.1	48.4	35.7
T98G	45.9	13.6	25.1
U251-MG	92.2	29.2	29.3
PD301	268.4	45.6	21.2
Compound 42			

U87-MG	85.9	51	28.6
T98G	348.4	25.4	31.6
U251-MG	129.1	43.2	30.2
PD301	616.9	162.5	34.9

The cell viability concentration response curves for compound **27** against the GBM cell lines and patient derived culture are shown in Figure 9; the curves for the other three analogues and Roscovitine are included in Figure S3-S6. Following 72 hours of treatment, cell viabilities at the highest concentration of **27** were reduced to < 5% of control for all cell lines except PD301 (cell viability ~16% of control). IC_{50} values after 72 hours for U87-MG, U251-MG and PD301 showed a decrease in comparison to 48 hours but for T98G an increase was observed. Nevertheless, the most affected cell line for **27** was T98G, following 48 hours with the IC_{50} value = 9.6 µM and following 72 hours, 11.7 µM. Therapeutic resistance, particularly for TMZ, is commonly observed for GBM patients as a result of O^6-methylguanine-DNA methyltransferase (MGMT) positive status. The T98G cell line is MGMT positive, so identification of compounds that show promise against this cell line could be effective in GBM with therapeutic resistance due to positive MGMT status.

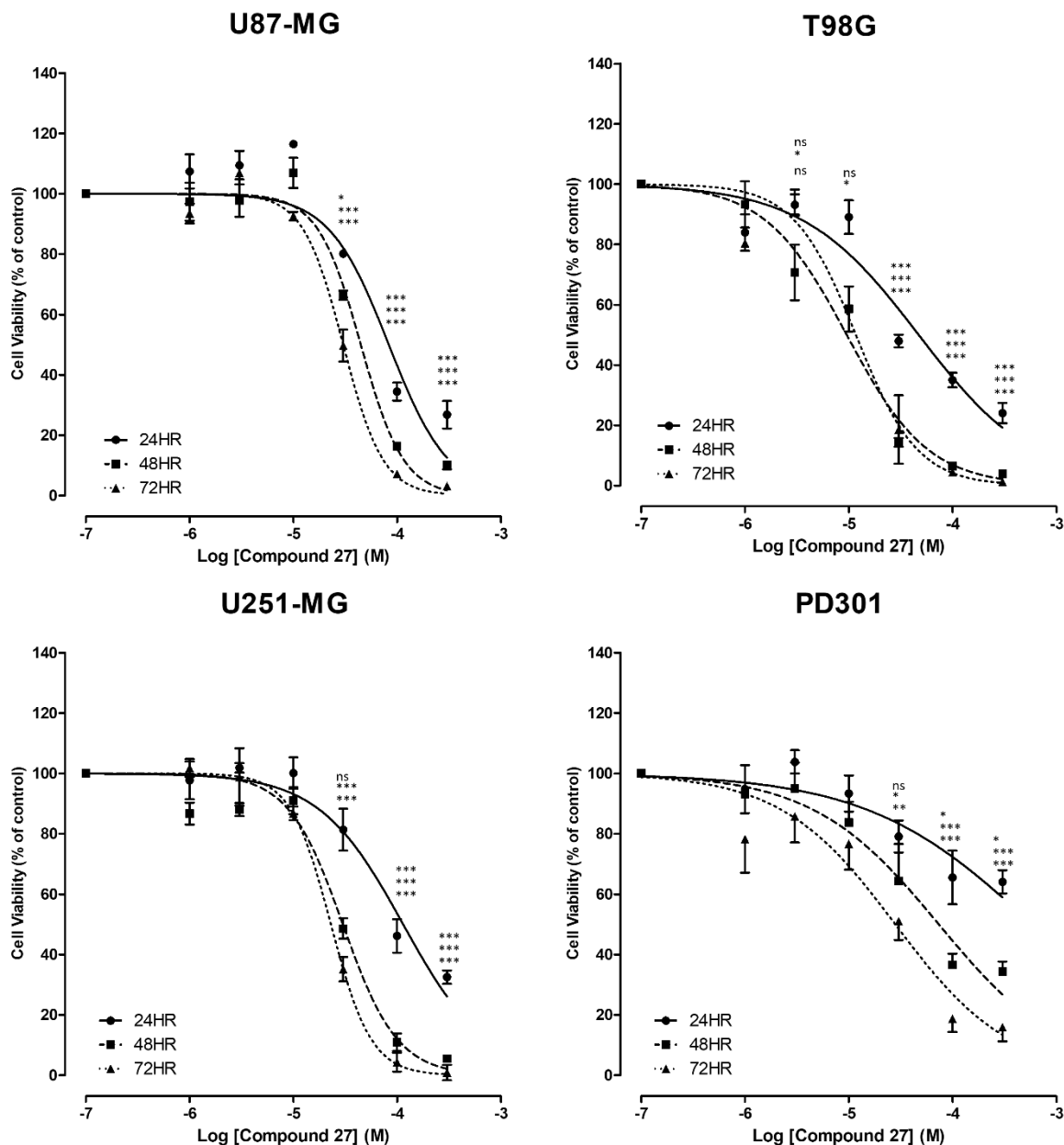**Figure 9**. Cell viability of the three glioblastoma cell lines, U87-MG, T98G, and U251-MG, and primary glioblastoma culture, PD301, following treatment with compound **27** at 24-, 48-, and 72-hours. Data obtained from mean ± SEM of three consecutive independent experiments. Significant effect observed between the treatment concentration and the control is noted above the concentration point in order of 24-, 48-, and 72- hours.

2.4 ADME Predictions

The predicted pharmacokinetics profiles of the four prioritized compounds (**4**, **27**, **36** and **42**) as calculated using QikProp are shown in Table 4. All compounds have predicted good oral

bioavailability, with no violations of Lipinski's 'rule of five' [52] or Jorgensen's 'rule of three',[53, 54] apart from a log S (water solubility) violation for compound **4**. The compounds also indicated some potential for permeability across the blood-brain barrier, considering the logBB values. A logBB = 0 suggests equal concentration of compound on either side of the blood-brain barrier. Proposed logBB cut-off values for potential CNS-active compounds vary, but thresholds as low as -1 have been suggested.[55, 56] One study which considered 18 approved CNS-active drugs, revealed a number of the compounds had QikProp logBB values in the range -1 to 0.[57] The predicted values of the four compounds here are in a similar range (-0.95 to -0.62). Polar surface area (PSA) is also an important parameter to consider. Ghose *et al.*[58] proposed a qualifying upper limit of 109 Å for QikProp calculated PSAs to favour brain permeation. The four compounds are just within this threshold. However, blood-brain barrier permeability would need closer consideration in future lead optimization studies.

Table 4. Predicted pharmacokinetics properties of prioritised compounds **4**, **27**, **36** and **42**.

Ligand	Lipinskis's Rule of Five and Violations (V)[a]					Jorgensen's Rule of Three and Violations (V)[a]				PSA [Å²][b]	log BB[c]
	MW [Da]	HBD[d]	HBA[e]	log P$_{(o/w)}$	V	Caco-2 [nm s^{-1}][f]	log S	NPM[g]	V		
	(<500)	(≤5)	(≤10)	(<5)		(>22)	(>--5.7)	(<7)			
4	449.5	3	7.90	3.8	0	1037	*-6.0*	4	1	101	-0.66
27	461.5	3	8.65	3.6	0	810	-5.6	5	0	109	-0.94
36	447.5	3	8.65	3.2	0	649	-5.3	5	0	106	-0.95
42	460.5	2	9.90	3.4	0	1551	-5.3	4	0	105	-0.62
Range[h]	130-725	0-6	02-20	-2-6.5	-	<25 poor; > 500 great	-6.5-0.5	1-8	-	7-200	-3.0-1.2

[a] Rules as listed in the columns, with any violations of the rules highlighted in italics. [b] PSA represents the van der Waals (polar) surface areas of N and O atoms [c] log BB: the predicted blood-brain barrier coefficient. [d] Number of hydrogen bond donors. [e] Number of hydrogen bond acceptors. [f] Caco-2 cell permeability. [g] Number of primary metabolites. [h] Range for 95% of known drugs - reference: QikProp version 3.5 User's Manual.

3. Conclusions

Discovery of drug-like selective kinase inhibitors has the potential to lead to novel new treatments for GBM and other cancers. There are more than 70 FDA approved kinase drugs, mainly for cancer, but none as yet for brain tumours. GBM has an urgent need for new therapeutic approaches, in the absence of any truly effective currently available treatment options. Here, for the first time, a CDK5 DFG-out model has been created using Meta-D and molecular dynamics simulations (in the absence of any crystallographic structure or evidence) to virtually screen for type-II inhibitors that bind to and stabilize the inactive conformation. Selection of a Phase I and II set of compounds led to the identification of four [pyrimidin-2-yl]amino-furo[3,2-b]-furyl-urea and [pyrimidin-2-yl]amino-furo[3,2-b]-furyl-amide analogues from the computational screen, the best of which were potent low micromolar inhibitors of CDK2, CDK5, CDK9 and GSK-3β, and nanomolar inhibitors of GSK-3α. These four compounds had predicted good oral bioavailability and log BB values that indicate potential for CNS-activity. All four compounds demonstrated highly promising effects on cell viability across GBM cell lines (U87-MG, T98G, and U251-MG) as well as a short-term patient derived culture (PD301), with $IC_{50}s$ generally in the range of $\sim 10 - 40$ μM observed following 72 hours treatment, and similar to those observed for Roscovitine ($IC_{50}s \sim 15$-19 μM) as a control. They appear to act, at least at the cellular level, independently of MGMT promoter methylation status, given their effectiveness against T98G. Specificity is a key issue in kinase inhibitor design. However, the multi-kinase inhibition demonstrated here are for kinases considered targets for GBM, meaning the compounds may tackle cancer through different mechanisms and potentially have synergistic effects. It can also reduce the possibility of developing drug resistance, a key issue with current GBM treatments and the large percentage of cases with tumour recurrence. [59, 60] These promising candidate compounds, given their initial therapeutic potential, can now

be used in further lead optimization studies against GBM, but additionally may have applications in other cancers.

4. Experimental

4.1 Computational Details

4.1.1 Ligand Preparation

All ligands were prepared for calculations using Schrödinger's Maestro and LigPrep v5.6.[29] All possible ligand ionization/tautomeric states at a pH of 7.0 ± 1.0 were generated, using the OPLS3e forcefield. The Biogenic subset of the ZINC15 database used for virtual screening consisted of 206,980 compounds that generated 271,474 chemical structures (with tautomers and ionization states) following LigPrep, ready for docking calculations. Qikprop v6.8 was used to calculate the ADME profiles of the ligands.[29]

4.1.2 Protein Preparation (DFG-in)

Using the 1.90 Å resolution solved crystallographic complex of CDK5 with (PDB code: 4AU8), the CDK5 protein was prepared for calculations using Schrödinger's Protein preparation wizard.[29] Hydrogens were added, bond orders assigned, water molecules deleted and any missing side-chains and loops added using Prime. Protonation states for acidic and basic residues were determined using the predicted PROPKA [61, 62] residue pKa values at pH 7.0. Subsequent optimization of residue hydroxyl groups, histidine protonation states and C/N atom flips, as well as sidechain O/N atom flips of Asn and Gln residues considered hydrogen bonding patterns. The system was then minimised using the OPLS3 forcefield [63] to converge heavy atoms to an RMSD within 0.3 Å of their crystallographic positions.

4.1.3 Metadynamics and Molecular Dynamics Simulations

Metadynamics

27

Using the prepared DFG-in model from PDB code: 4AU8 with cognate ligand deleted, the Desmond system builder within Schrödinger's' Maestro was used to create the system for MetaD simulations.[25] The TIP3P model (10,150 water molecules) was employed as the solvent model in an orthorhombic box with sides a = 67.704 Å, side b = 61.914 Å, side c = 86.894 Å (volume = 363,151 Å^3), with box edges 10 Å from the protein. The system was neutralised by addition of a Cl$^-$ atom, with the final simulation model consisting of 35,121 atoms. Heavy atom bond lengths with hydrogen atoms and internal geometries of water molecules were constrained with the SHAKE algorithm. For the Meta-D simulation, one collective variable (CV) was used, defined as the distance between the centre of mass (COM) of Phe145 side-chain and the Cα atom of Gly113, with the wall capped at 23 Å and Gaussian width set to 0.05 Å. The CV was selected adapting for CDK5 a successful Meta-D approach to creating a DFG-out model for GSK-3β.[26] Clustal Omega multiple sequence alignment as well as structural superimposition/comparisons of CDK5 and GSK-3β (PDB:2OW3) identified the equivalent residues. Following the initial default relaxation/equilibration stage, the MetaD simulation was ran for 50 ns in the NPT ensemble (T = 300 K, P = 1 atm), the height of the Gaussian potential was 0.03 kcal/mol, and the Gaussians deposited every 0.09 ps. A total of 1000 frames were saved (every 50 ps). The RESPA integrator was used with a time step of 2.0 fs for bonded and near interactions and 6.0 fs for far interactions. Periodic boundary conditions (PBC) were employed and a cut-off of 9.0 Å for non-bond interactions; electrostatic interactions treated using Particle Mesh Ewald (PME) method. The OPLS3e forcefield [63] was used and simulation performed using Desmond.[25]

Molecular Dynamics

The DFG-out model created using MetaD and with sorafenib subsequently docked was used as input for molecular dynamics (MD) refinement using Desmond 2018-4. The Desmond system builder was again used to soak the complex with a pre-equilibrated TIP3P solvent model

28

(10,871 waters) in an orthorhombic box with side lengths $a = 62.435$ Å, side $b = 68.213$ Å and side $c = 91.853$ Å (box volume = 391,189 Å^3) and a 10 Å buffer to the box sides. The structure was neutralised by the addition of a Cl$^-$ atom, placed beyond 25 Å of the sorafenib ligand and the forcefield used was the OPLS3e. The final system consisted of 37,332 atoms. The specific settings in terms of initial equilibration, employment of SHAKE algorithm constraints, PBCs, forcefield (OPLS3e), treatment of non-bond interactions was as for the MetaD simulation outlined above. The production run was a 100 ns in the NPT ensemble at a temperature of 300K and pressure 1 atm, using the NPT ensemble. Trajectory energy data and atomic coordinates were collected every 1.2 and 5.0 ps, respectively. To account for the equilibration of the system, the first 20 ns of the 100 ns trajectory was spliced out. The remaining trajectory frames were clustered into ten clusters using Desmond Trajectory Clustering with the hierarchical cluster linkage method, and a representative taken from the most populated cluster to be used as the final DFG-out structure for virtual screening.

4.1.4 Docking Calculations

DFG-out conformation: For the docking calculations with Glide v9.1[29, 64] the shape and properties of the CDK5 binding site was mapped onto grids with dimensions of ~ 29.7 Å × 29.7 Å x 29.7 Å centred on sorafenib; in the initial docking of sorafenib to the MetaD output DFG-out model, the centroid based on hinge region residues Glu81 - Cys83 and the DFG loop residue Asp144 was used. Glide docking was performed in SP mode with mainly default parameters employed that included default OPLS3e [63] atomic charges and van der Waals scaling (0.8) for non-polar ligand atoms to incorporate modest induced-fit effects. The ligand sampling was set to flexible with both sample nitrogen inversions and sample ring conformations selected; Epik state penalties were included to give the docking scores. Constraints during docking were applied to ensure classical type-II hydrogen bond interactions form with the hinge region Glu81 and Cys83 backbones (at least one from three), αC helix Glu51 side chain and activation loop

29

Asp144 backbone. Post-docking minimisation and strain correction terms were applied, with the top-ranked pose per ligand saved and ligands ranked based on the docking score.

DFG-in conformation: For the docking calculations to CDK5 DFG-in conformation, prepared protein PDB code: 4AU8 (section 4.1.2.), the same general docking settings used for DFG-out docking were applied, except hydrogen bond constraints were only used for the ATP-binding site hinge region and the docking grid based on the centroid of the native ligand had dimensions of ~ 23.4 Å × 23.4 Å x 23.4 Å.

4.2 Experimental Details

4.2.1 *In Vitro* Isolated Enzyme Binding Assays

The *in vitro* binding assay validation of the predicted CDK5 inhibitors was performed using a specialist service from the MRC Protein Phosphorylation & Ubiquitylation Unit and the 'International Centre for Kinase Profiling' at the University of Dundee (https://www.kinase-screen.mrc.ac.uk/). Candidate inhibitor compounds (Phase I and II) were purchased from Analyticon discovery, Biosynth, Mcule and Vitas-M (*c.f.* Supplementary Information, Excel file). Initially, single concentration screening of the compounds against CDK5/p35 at 50 µM was performed. Inhibitory activities were determined based on maximal activities measured in absence of the inhibitor. Candidates which demonstrated best inhibition were selected for IC$_{50}$ determinations. For the kinase selectivity profiling, compounds were assayed at a single concentration (50 µM) against a panel of kinases (CDK2, CDK9, CDK5/p35, ERK1, ERK2, GSK-3α, GSK-3β, PKA, PKBα, PKBβ, PKCα and PKCγ). Further IC$_{50}$s were determined for CDK2, CDK9, GSK-3α and GSK-3β for the four selected hit compounds **4**, **27**, **36** and **42** (purities > 95% by HPLC, except for **27** at 91%). All binding assay experiments were performed in duplicate.

4.2.2 *In Vitro* Glioblastoma Assays

Three glioblastoma cell lines were used for the cell viability experiments (U-87 MG, T98G, and U-251 MG). The U-251 MG cells were obtained from the University of Wolverhampton and the remaining cell lines from the American Type Culture Collection. Short term patient derived cells (PD301) were also used, acquired from the Brain Tumour North West tissue bank. Cell lines were maintained in Eagles Minimum Essential Media (EMEM), supplemented with L-glutamine (2mM), 1% Non-Essential Amino Acids (NEAA), sodium pyruvate (1mM) and 10% Foetal Bovine Serum (FBS), all purchased from Gibco. Cells were grown at 37°C in a humidified atmosphere maintained at 5% CO_2. Cells were initially seeded at a density of 1×10^3 cells/well in 96-well plates and cultured for 24 hour prior to treatment with the compounds (1, 3, 10, 30, 100 and 300 µM). The concentration of DMSO vehicle used did not exceed 0.5%, which was not cytotoxic to the cells. Cell viability was measured at 24-, 48- and 72- hour post-treatment, using PrestoBlue® at an excitation/emission of 535/612nm. Roscovitine (purity > 95% by HPLC) was used as a control for comparison with the four selected hit compounds (**4**, **27**, **36** and **42**) tested. For statistical analysis SPSS was used, with a two-way ANOVA (analysis of variance) and a Bonferroni post-hoc test used to identify significant differences between experimental groups. Significance between the time points as well as treatment concentrations were determined. *P*- values ≤ 0.05 were considered as statistically significant with significance indicated in figures as: ns $p > 0.05$, * $p \leq 0.05$, ** $p \leq 0.01$, and *** $p \leq 0.001$.

Supporting Information

The Supporting Information is available free of charge. Supplementary Tables and Figures from calculations and cell viability experiments; HPLC-chromatograms for the four identified lead compounds (**4**, **27**, **36** and **42**); molecular strings formula (SMILES), IUPAC names and % purities of all compounds (CSV); 3D hydrogen-suppressed atomic model of the CDK5 DFG-

out refined complex with sorafenib – authors will release the atomic coordinates upon article publication.

Acknowledgements

Corresponding Author

* Joseph M. Hayes; email: jhayes@uclan.ac.uk

Abbreviations

AD, Alzheimer's Disease; ADME, Absorption, Distribution, Metabolism, Excretion; CDK, Cyclin-Dependent Kinase; COM, Centre of Mass; CV, Collective Variable, DFG, Asp – Phe – Glu; EMEM, Eagles Minimum Essential Media; FBS, Foetal Bovine Serum; GBM, Glioblastoma; GSC, Glioma Stem Cell; HBA, Hydrogen Bond Acceptor; HBD, Hydrogen Bond Donor; MD, Molecular Dynamics; MetaD, Metadynamics; MGMT, O6-methylguanine-DNA methyltransferase; MKI, Multiple Kinase Inhibitors; NEAA, Non-Essential Amino Acids; PAINS, Pan Assay Interference Compounds; PBC, Periodic Boundary Conditions; PME, Particle Mesh Ewald; PSA, Polar Surface Area; SAR, Structure-Activity Relationship; TMZ, Temozolomide.

References

(1) Krex, D.; Klink, B.; Hartmann, C.; von Deimling, A.; Pietsch, T.; Simon, M.; Sabel, M.; Steinbach, J. P.; Heese, O.; Reifenberger, G.; et al. Long-term survival with glioblastoma multiforme. *Brain* **2007**, *130* (10), 2596-2606.

(2) Lee, S. Y. Temozolomide resistance in glioblastoma multiforme. *Genes & Diseases* **2016**, *3* (3), 198-210.

(3) Manning, G.; Whyte, D. B.; Martinez, R.; Hunter, T.; Sudarsanam, S. The protein kinase complement of the human genome. *Science* **2002**, *298* (5600), 1912-1934.

(4) Roufayel, R.; Murshid, N. CDK5: Key regulator of apoptosis and cell survival. *Biomedicines* **2019**, *7* (4), 88.

(5) Yushan, R.; Wenjie, C.; Suning, H.; Yiwu, D.; Tengfei, Z.; Madushi, W. M.; Feifei, L.; Changwen, Z.; Xin, W.; Roodrajeetsing, G.; et al. Insights into the clinical value of cyclin-dependent kinase 5 in glioma: A retrospective study. *World J. Surg. Oncol.* **2015**, *13* (1), 223-223.

(6) Do, P. A.; Lee, C. H. The role of CDK5 in tumours and tumour microenvironments. *Cancers* **2021**, *13* (1), 1-27.

(7) Zhou, Y.; Wang, X.; Lv, P.; Yu, H.; Jiang, X. CDK5 Knockdown inhibits proliferation and induces apoptosis and cell cycle arrest in human glioblastoma. *J. Cancer* **2021**, *12* (13), 3958-3966.

(8) Mukherjee, S.; Tucker-Burden, C.; Kaissi, E.; Newsam, A.; Duggireddy, H.; Chau, M.; Zhang, C.; Diwedi, B.; Rupji, M.; Seby, S.; et al. CDK5 Inhibition resolves PKA/cAMP-independent activation of CREB1 signaling in glioma stem cells. *Cell Rep.* **2018**, *23* (6), 1651-1664.

(9) Tabouret, E.; Wang, H.; Amin, N.; Jung, J.; Appay, R.; Cui, J.; Song, Q.; Cardone, A.; Park, D. M.; Gilbert, M. R.; et al. TP5, a peptide inhibitor of aberrant and hyperactive CDK5/p25: A novel therapeutic approach against glioblastoma. *Cancers* **2020**, *12* (7), 1-16.

(10) Cicenas, J.; Cicenas, E. Multi-kinase inhibitors, AURKs and cancer. *Medical Oncol.* **2016**, *33* (5), 43.

(11) Garuti, L.; Roberti, M.; Bottegoni, G. Multi-kinase inhibitors. *Curr. Med. Chem.* **2015**, *22* (6), 695-712.

(12) Xie, Q.; Wu, Q.; Kim, L.; Miller, T. E.; Liau, B. B.; Mack, S. C.; Yang, K.; Factor, D. C.; Fang, X.; Huang, Z.; et al. RBPJ maintains brain tumor-initiating cells through CDK9-mediated transcriptional elongation. *J. Clin. Invest.* **2016**, *126* (7), 2757-2772.

33

(13) Adelman, K.; Lis, J. T. Promoter-proximal pausing of RNA polymerase II: emerging roles in metazoans. *Nature reviews. Genetics* **2012**, *13* (10), 720-731.

(14) Ancker, O. V.; Krüger, M.; Wehland, M.; Infanger, M.; Grimm, D. Multikinase inhibitor treatment in thyroid cancer. *Int. J. Mol. Sci.* **2019**, *21* (1), 10.

(15) Roskoski, R. Properties of FDA-approved small molecule protein kinase inhibitors: A 2023 update. *Pharmacol. Res.* **2023**, *187*, 106552-106552.

(16) Blanc, J.; Geney, R.; Menet, C. Type II Kinase Inhibitors: An opportunity in cancer for rational design. *Anti-cancer Agents Med. Chem.* **2013**, *13* (5), 731-747.

(17) Treiber, Daniel K.; Shah, Neil P. Ins and outs of kinase DFG motifs. *Chem. Biol.* **2013**, *20* (6), 745-746.

(18) Copeland, R. A.; Pompliano, D. L.; Meek, T. D. Drug-target residence time and its implications for lead optimization. *Nat. Rev.. Drug Discovery* **2006**, *5* (9), 730-739.

(19) Willemsen-Seegers, N.; Uitdehaag, J. C. M.; Prinsen, M. B. W.; de Vetter, J. R. F.; de Man, J.; Sawa, M.; Kawase, Y.; Buijsman, R. C.; Zaman, G. J. R. Compound selectivity and target residence time of kinase inhibitors studied with surface plasmon resonance. *J. Mol. Biol.* **2017**, *429* (4), 574-586.

(20) Kufareva, I.; Abagyan, R. Type-II kinase inhibitor docking, screening, and profiling using modified structures of active kinase states. *J. Med. Chem.* **2008**, *51* (24), 7921-7932.

(21) Davis, M. I.; Hunt, J. P.; Herrgard, S.; Ciceri, P.; Wodicka, L. M.; Pallares, G.; Hocker, M.; Treiber, D. K.; Zarrinkar, P. P. Comprehensive analysis of kinase inhibitor selectivity. *Nat. Biotech.* **2011**, *29* (11), 1046-1051.

(22) Newman, D. J.; Cragg, G. M. Natural products as sources of new drugs over the nearly four decades from 01/1981 to 09/2019. *J. Nat. Prod.* **2020**, *83* (3), 770-803.

(23) Mali, S. B. Cancer treatment: Role of natural products. Time to have a serious rethink. *Oral Oncol. Rep.* **2023**, *6*, 100040.

(24) Sterling, T.; Irwin, J. J. ZINC 15 – Ligand discovery for everyone. *J. Chem. Inf. Model.* **2015**, *55* (11), 2324-2337.

(25) Desmond Molecular Dynamics System, D. E. Shaw Research, New York, NY, 2018-4. Maestro-Desmond Interoperability Tools, Schrödinger, New York, NY, 2018.

(26) Balasubramaniam, M.; Mainali, N.; Bowroju, S. K.; Atluri, P.; Penthala, N. R.; Ayyadevera, S.; Crooks, P. A.; Shmookler Reis, R. J. Structural modeling of GSK3β implicates the inactive (DFG-out) conformation as the target bound by TDZD analogs. *Sci. Rep.* **2020**, *10* (1), 18326-18326.

(27) Vijayan, R. S. K.; He, P.; Modi, V.; Duong-Ly, K.; Ma, H.; Peterson, J. R.; Dunbrack, R. L.; Levy, R. M. Conformational Analysis of the DFG-Out kinase motif and biochemical profiling of structurally validated Type II inhibitors. *J. Med. Chem.* **2015**, *58* (1), 466-479.

(28) Davies, M. P.; Benitez, R.; Perez, C. n.; Jakupovic, S.; Welsby, P.; Rzepecka, K.; Alder, J.; Davidson, C.; Martinez, A.; Hayes, J. M. Structure-based design of potent selective nanomolar Type-II inhibitors of glycogen synthase kinase-3β. *J. Med. Chem.* **2021**, *64* (3), 1497-1509.

(29) Schrödinger Release, 2020-4. Maestro; Schrödinger LLC: New York, NY, 2020.

(30) Modi, V.; Dunbrack, R. L. Defining a new nomenclature for the structures of active and inactive kinases. *Proc. Nat. Acad. Sci.* **2019**, *116* (14), 6818-6827.

(31) Zhao, Z.; Wu, H.; Wang, L.; Liu, Y.; Knapp, S.; Liu, Q.; Gray, N. S. Exploration of type II binding mode: A privileged approach for kinase inhibitor focused drug discovery? *ACS Chem. Biol.* **2014**, *9* (6), 1230.

(32) Stewart, H. L.; Bon, M.; Wills, C.; Martin, M. P.; Wang, L. Z.; Mackenzie, E. S.; Waddell, P. G.; Waring, M. J. Conformational study into N-alkyl-N′-aryl ureas to inform drug discovery. *Bioorg. Med. Chem.* **2023**, *91*, 117387-117387.

(33) Loeffler, J. R.; Ehmki, E. S. R.; Fuchs, J. E.; Liedl, K. R. Kinetic barriers in the isomerization of substituted ureas: implications for computer-aided drug design. *J. Comput.-Aid. Mol. Des.* **2016**, *30* (5), 391-400.

(34) Zeb, A.; Son, M.; Yoon, S.; Kim, J. H.; Park, S. J.; Lee, K. W. Computational simulations identified two candidate inhibitors of CDK5/p25 to abrogate tau-associated neurological disorders. *Comput. Struct. Biotech. J.* **2019**, *17*, 579-590.

(35) Baumli, S.; Hole, A. J.; Noble, M. E. M.; Endicott, J. A. The CDK9 C-helix exhibits conformational plasticity that may explain the selectivity of CAN508. *ACS Chem. Biol.* **2012**, *7* (5), 811-816.

(36) Wang, J.; Yang, T.; Xu, G.; Liu, H.; Ren, C.; Xie, W.; Wang, M. Cyclin-dependent kinase 2 promotes tumor proliferation and induces radio resistance in glioblastoma. *Trans. Oncol.* **2016**, *9* (6), 548-556.

(37) Juric, V.; Murphy, B. Cyclin-dependent kinase inhibitors in brain cancer: current state and future directions. *Cancer Drug Resist.* **2020**, *3* (1), 48-62.

(38) Ranjan, A.; Pang, Y.; Butler, M.; Merchant, M.; Kim, O.; Yu, G.; Su, Y.-T.; Gilbert, M. R.; Levens, D.; Wu, J. Targeting CDK9 for the treatment of glioblastoma. *Cancers* **2021**, *13* (12), 3039.

35

(39) Nakada, M.; Toshinari, M.; Ilya V. P.; Yutaka, H.; Jun-ichiro, H. The pivotal roles of GSK3β in glioma biology. In *Molecular Targets of CNS Tumors*; Miklos, G., Ed.; IntechOpen: Rijeka, 2011; pp 567-590.

(40) Alexander, L. T.; Möbitz, H.; Drueckes, P.; Savitsky, P.; Fedorov, O.; Elkins, J. M.; Deane, C. M.; Cowan-Jacob, S. W.; Knapp, S. Type II inhibitors targeting CDK2. *ACS Chem. Biol.* **2015**, *10* (9), 2116-2125.

(41) Yao, H.-B.; Shaw, P.-C.; Wong, C.-C.; Wan, D. C.-C. Expression of glycogen synthase kinase-3 isoforms in mouse tissues and their transcription in the brain. *J. Chem. Neuroanatomy* **2002**, *23* (4), 291-297.

(42) Domoto, T.; Uehara, M.; Bolidong, D.; Minamoto, T. Glycogen synthase kinase 3β in cancer biology and treatment. *Cells* **2020**, *9* (6), 1388.

(43) Lauretti, E.; Dincer, O.; Praticò, D. Glycogen synthase kinase-3 signaling in Alzheimer's disease. *Biochim. et Biophys/ Acta. Mol. Cell Res.* **2020**, *1867* (5), 118664-118664.

(44) Phiel, C. J.; Wilson, C. A.; Lee, V. M. Y.; Klein, P. S. GSK-3alpha regulates production of Alzheimer's disease amyloid-beta peptides. *Nature* **2003**, *423* (6938), 435-439.

(45) Silva-García, O.; Cortés-Vieyra, R.; Mendoza-Ambrosio, F. N.; Ramírez-Galicia, G.; Baizabal-Aguirre, V. M. GSK3α: An important paralog in neurodegenerative disorders and cancer. *Biomolecules* **2020**, *10* (12), 1-23.

(46) Carter, Y. M.; Kunnimalaiyaan, S.; Chen, H.; Gamblin, T. C.; Kunnimalaiyaan, M. Specific glycogen synthase kinase-3 inhibition reduces neuroendocrine markers and suppresses neuroblastoma cell growth. *Cancer Biol. Ther.* **2014**, *15* (5), 510-515.

(47) Amaral, B.; Capacci, A.; Anderson, T.; Tezer, C.; Bajrami, B.; Lulla, M.; Lucas, B.; Chodaparambil, J. V.; Marcotte, D.; Kumar, P. R.; et al. Elucidation of the GSK3α structure informs the design of novel, paralog-selective inhibitors. *ACS Chem. Neurosci.* **2023**, *14* (6), 1080-1094.

(48) Canduri, F.; de Azevedo, W. F. Structural basis for interaction of inhibitors with cyclin-dependent kinase 2. *Curr. Comput.-Aided Drug Des.* **2005**, *1* (1), 53-64.

(49) Cicenas, J.; Kalyan, K.; Sorokinas, A.; Stankunas, E.; Levy, J.; Meskinyte, I.; Stankevicius, V.; Kaupinis, A.; Valius, M. Roscovitine in cancer and other diseases. *Annals Translat. Med.* **2015**, *3* (10).

(50) Banelli, B.; Daga, A.; Forlani, A.; Allemanni, G.; Marubbi, D.; Pistillo, M. P.; Profumo, A.; Romani, M. Small molecules targeting histone demethylase genes (KDMs) inhibit growth of temozolomide-resistant glioblastoma cells. *Oncotarget* **2017**, *8* (21), 34896-34910.

(51) Friedman, H. S.; Kerby, T.; Calvert, H. Temozolomide and treatment of malignant glioma. *Clin. Cancer Res.* **2000**, *6* (7), 2585-2597.

(52) Lipinski, C. A.; Lombardo, F.; Dominy, B. W.; Feeney, P. J. Experimental and computational approaches to estimate solubility and permeability in drug discovery and development settings. *Adv. Drug Deliv. Rev.* **1997**, *23* (1), 3-25.

(53) Jorgensen, W. L.; Duffy, E. M. Prediction of drug solubility from Monte Carlo simulations. *Bioorg. Med. Chem. Lett.* **2000**, *10* (11), 1155-1158.

(54) Jorgensen, W. L.; Duffy, E. M. Prediction of drug solubility from structure. *Adv. Drug Deliv. Rev.* **2002**, *54* (3), 355-366.

(55) Carpenter, Timothy S.; Kirshner, Daniel A.; Lau, Edmond Y.; Wong, Sergio E.; Nilmeier, Jerome P.; Lightstone, Felice C. A method to predict blood-brain barrier permeability of drug-like compounds using molecular dynamics simulations. *Biophys. J.* **2014**, *107* (3), 630-641.

(56) Luco, J. M. Prediction of the brain-blood distribution of a large set of drugs from structurally derived descriptors using partial least-squares (PLS) modeling. *J. Chem. Inf. Comput. Sci.* **1999**, *39* (2), 396-404.

(57) Emmerich, T. D.; Hayes, J. M. In silico-motivated discovery of novel potent glycogen synthase-3 inhibitors: 1-(Alkyl/arylamino)-3H-naphtho[1,2,3-de]quinoline-2,7-dione identified as a scaffold for kinase inhibitor development. *Pharmaceuticals* **2023**, *16* (5), 661.

(58) Ghose, A. K.; Herbertz, T.; Hudkins, R. L.; Dorsey, B. D.; Mallamo, J. P. Knowledge-based, central nervous system (CNS) lead selection and lead optimization for CNS drug discovery. *ACS Chem. Neurosci.* **2012**, *3* (1), 50-68.

(59) Dymova, M. A.; Kuligina, E. V.; Richter, V. A. Molecular mechanisms of drug resistance in glioblastoma. *Int. J. Mol. Sci.* **2021**, *22* (12), 6385.

(60) Olivier, C.; Oliver, L.; Lalier, L.; Vallette, F. M. Drug resistance in glioblastoma: The two faces of oxidative stress. *Front. Mol. Biosci.* **2021**, *7*, 620677-620677.

(61) Olsson, M. H. M.; SØndergaard, C. R.; Rostkowski, M.; Jensen, J. H. PROPKA3: Consistent treatment of internal and surface residues in empirical pKa predictions. *J. Chem. Theory Comput.* **2011**, *7* (2), 525-537.

(62) Søndergaard, C. R.; Olsson, M. H. M.; Rostkowski, M.; Jensen, J. H. Improved treatment of ligands and coupling effects in empirical calculation and rationalization of pKa values. *J. Chem. Theory Comput.* **2011**, *7* (7), 2284-2295.

(63) Harder, E.; Damm, W.; Maple, J.; Wu, C.; Reboul, M.; Xiang, J. Y.; Wang, L.; Lupyan, D.; Dahlgren, M. K.; Knight, J. L.; et al. OPLS3: A force field providing broad coverage of drug-like small molecules and proteins. *J. Chem. Theory Comput.* **2016**, *12* (1), 281-296.

(64) Friesner, R. A.; Banks, J. L.; Murphy, R. B.; Halgren, T. A.; Klicic, J. J.; Mainz, D. T.; Repasky, M. P.; Knoll, E. H.; Shelley, M.; Perry, J. K.; et al. Glide: A new approach for rapid, accurate docking and scoring. 1. Method and assessment of docking accuracy. *J. Med. Chem.* **2004**, *47* (7), 1739-1749.